Regular Article

PHYSICAL CHEMISTRY RESEARCH
Published by the
Iranian Chemical Society
www.physchemres.org
info@physchemres.org

Phys. Chem. Res., Vol. 12, No. 2, 383-392, June 2024
DOI: 10.22036/pcr.2023.407583.2378

Synthesis of Zinc Oxide Nanoparticles by Citrus Limon as an Effective Photoanode for Dye-Sensitized Solar Cells

R. Naresh Muthu*

Department of Physics, J P College of Arts and Science, Tenkasi-627852, Tamil Nadu
(Affiliated to Manonmaniam Sundaranar University, Tirunelveli, Tamil Nadu)
(Received 18 July 2023, Accepted 30 August 2023)

ZnO nanoparticles are prepared with lime juice by the green, facile solution combustion method and act as a photoanode for DSSC fabrication. The structural and morphological features of ZnO nanoparticles are examined *via* XRD, FTIR, UV-Vis, DLS, and SEM. The XRD detects defect-free wurtzite hexagonal structure with a crystallite size of ~16.28 nm. SEM image reveals a spherical morphology with a uniform spreading of ZnO nanoparticles (~45 nm). UV-Vis analysis exhibited high absorbance in the UV (~200 to 400 nm) and vital transparency in the visible region (~400 to 600 nm). The band gap (3.07 eV) is estimated and is blue-shift and associated with the bulk of the ZnO (3.37 eV) because of the impact of quantum confinement. The doctor blade approach is adopted to prepare photoanode. ZnO-based DSSC is constructed, wherein Pt is the counter electrode, with an iodine redox couple as the electrolyte and N719 dye utilized as a sensitizer. Photovoltaic performance (V_{oc}, J_{sc}, η, and *FF*) of the fabricated FTO/ZnO-N719 dye/iodide redox coupled electrolyte/Pt/FTO device is studied. The maximum (PCE) η 3.7447% is achieved with a maximum V_{oc} ~ 0.734 mV, J_{sc} ~ 9.768 mA cm^{-2}, and FF ~ 0.5223. Hence, synthesized ZnO nanoparticles may be an excellent photoanode material for DSSC application.

Keywords: Semiconductors, ZnO, Nanoparticles, Solution combustion method, Dye-sensitized solar cell

INTRODUCTION

Nowadays, transition metal oxides such as V_2O_5 (vanadium pentoxide), ZnO (zinc oxide), ZrO_2 (zirconium dioxide), TiO_2 (titanium dioxide), and WO_3 (tungsten trioxide) with nanostructure have attracted more attention in many areas of technology [1]. One of them, ZnO, is the most gifted II-VI compound semiconductor (n-type). ZnO, an inorganic oxide, is classified as a transparent conductive oxide. ZnO nanoparticle exhibits a direct band gap (~ 3.22 eV), high excitation binding energy (~ 60 meV), and electrical conductivity (~103 to 104 S cm^{-1}) at room temperature (RT). Owing to their low carrier concentration and oxygen vacancies, ZnO nanoparticles are highly resistive at RT [2,3]. ZnO nanoparticles have been at the forefront of research in various fields owing to their unique electrical, mechanical, and optical assets (stability, excellent electron mobility, high conductivity, and high electron affinity) [4]. Because of these features, ZnO nanoparticles have potentially been applied in various sectors like gas sensors, textiles, photoelectrode, water purification, cosmetics, photocatalysis, solar cells, light-emitting devices, and biomedical applications (targeted drug delivery, bioimaging, anticancer and wound healing) [5-7].

Photovoltaic (PV) translation of solar energy is a critical alarm of today's world to part to meet the energy requirement through an environmentally non-polluting mechanism that partially solar cell converts sunlight into electricity directly [8]. DSSCs (Dye-sensitized solar cells) have recently occurred as the most favorable photovoltaics in recent years for mass production. DSSCs are based on an electrolyte, counter electrode, and oxide semiconductors (photoanode) absorbed by organic dyes or metal-organic complex dyes to achieve efficient solar-energy conversion [9]. Due to their

*Corresponding author. E-mail: rnaresh7708@gmail.com

simple fabrication methods, flexibility, and potential low manufacture costs compared with the most versatile silicon-based photovoltaic devices, they suffer from the efficiency and stability of DSSCs [10,11].

The DSSC device, porous structured semiconductor oxide (TiO_2 and ZnO), is investigated as the photosensitized anode material owing to its high surface area for dye molecule adsorption. The DSSCs are fabricated using porous TiO_2 as a photoanode, increasing power conversion efficiency by 13% [12]. However, a further rise in the conversion power efficiency (PCE) is constrained by recombination among electrons and electron-accepting species in the electrolyte and energy loss due to the oxidization of dye molecules through the charge transport mechanism. In recent years, ZnO-based DSSC has emerged as an alternative to TiO_2. ZnO is preferred as a photoanode semiconductor material because of its suitable energy band, high electron mobility, longer electron lifetime, fast electron transport, and less recombination loss [13]. The ZnO nanotube (as a photoanode) using N719 as sensitization revealed 1.18% PCE [14]. Keis *et al.* [15] prepared ZnO nanoparticles through the compression method, exhibiting a high PCE of 5%. ZnO microspheres prepared by Li *et al.* indicated a PCE of 5.16% [16]. ZnO is much lower than TiO_2 due to the size and shape restraint compared to the photoconversion efficiencies.

Various approaches are used to synthesize ZnO nanoparticles, like chemical precipitation, sol-gel, solution combustion, hydrothermal, solvothermal, solution-free mechanochemical methods, sonochemical, microwave, chemical bath deposition (CBD), *etc*. These approaches require unique, expensive instrumental setups, high temperatures, and toxic chemicals that are unfriendly to the environment [17-23]. The solution combustion method is attracting much attention for preparing ZnO nanoparticles owing to its accessibility, cost-effectiveness, and eco-friendliness compared to other approaches [3].

This research is to green synthesize ZnO nanoparticles by the solution combustion route using citrus limon (lemon) extract and investigate the photoconversion efficiency of the DSSC device. Different analytical techniques like XRD, FTIR, UV-Vis, DLS, and SEM are used to examine the synthesized ZnO nanoparticles' structural, chemical composition, optical properties, band gap, and morphology.

The devices were fabricated by coating the synthesized ZnO nanoparticles paste onto the FTO substrates *via* the doctor blade technique and acting as a photoanode. In contrast, Pt played the role of the counter electrode. The electrolyte function in the DSSC was evaluated by introducing $an\ I_3^-/I^-$redox couple. The photovoltaic behavior of the constructed DSSC device, FTO/ZnO-N719 dye/iodide redox coupled electrolyte/Pt/FTO was studied in terms of V_{oc}, J_{sc}, η, and *FF* from the J-V curve. The maximum photoconversion efficiency of (η) ZnO-based DSSC was revealed a 3.7447% and quite impressive related to the various preparation routes of ZnO nanoparticles as photoanode. Thus, the better performance of ZnO-based photoanode is ascribed to the low band gap of ZnO nanoparticles by facile solution-combustion route through the citrus lemon extract. Therefore, the constructed FTO/ZnO - N719 dye/iodide redox coupled electrolyte/Pt/FTO dye-sensitized solar cells may be an efficient solar cell device.

EXPERIMENTAL

Materials

Himedia provided the $Zn(NO_3)_2.6H_2O$ (Zinc nitrate hexahydrate). FTO (Fluorine-doped tin oxide) substrates, 99% acetylacetone, 99% pluronic 123, and Triton-X-100 were received from Sigma Aldrich. N719 dye, iodolyte (HI-30), and plastisol T/SP were obtained from Solaronix SA. Merck supplied ethanol (99%), Tetrabutanol, and acetonitrile. All analytical grade (AR) chemicals were utilized without further treatment. DI (Deionized) water was used during the present research work.

Preparation of ZnO Nanoparticles

The ZnO nanoparticles were prepared by solution combustion route using $Zn(NO_3)_2.6H_2O$ (oxidation agent) and afresh synthesized citrus limon juice (biofuel). In the synthesis, 1 M of $Zn(NO_3)_2.6H_2O$ was dissolved in DI water and stirred at RT for 5 min. An appropriate amount of freshly prepared citrus limon juice was added gradually. A magnetic stirrer continued stirring the above solution until it became homogenized. After that, the obtained homogeneous solution was then kept at a hot plate (100 °C) [24-26]. The resultant end product was well grounded by mortar and pestle. Then, the residue was shifted into the muffle furnace and annealed

at 500 °C (3 h). Finally, fine ZnO nanoparticle powder was obtained and used for further analysis.

Preparation of ZnO Photoanode

The doctor blade method was utilized to construct the ZnO photoanode [27-29]. Initially, FTO glass substrates were cleaned with water (DI), acetone, ethanol, and isopropyl alcohol using the ultrasonic treatment for 15 min and then dried in a vacuum. A 1 g of synthesized ZnO nanoparticles was mixed with acetylacetone and ground well with mortar and pestle assistance until a paste was attained. Then, the paste was stirred with DI water and ethanol (1:1) volume solutions. Triton-X was added drop by drop to form a homogenous paste. In the film coating, the edges of the precleaned FTO substrate were enclosed with scotch tape (adopt the thickness) and an active area of ~1cm^2 of the film. Using a glass rod, the prepared paste was coated uniformly onto the washed FTO substrate and reserved at room temperature (15 min) to evaporate the solvent. Then the ZnO-deposited FTO substrate was annealed at 450 °C (30 min) to evaporate the binder materials. The measured thickness of the synthesized ZnO nanoparticles coated with FTO substance was ~15 μm, and a thickness profilometer measured it. The prepared ZnO photoanode was soaked in N719 dye in tertbutanol and acetonitrile (1:1 volume) solution for 1 day in the ark atmosphere at RT. Later, the substrates were detached from the N719 dye and cleaned with ethyl alcohol to remove unabsorbed dye from the ZnO-coated FTO substrate surface and dried in the air. This N719 dye-absorbed FTO/ZnO substrate acted as the photoanode for DSSC device fabrication.

Preparation of Counter Electrode and Electrolyte

For the construction of DSSC, electrolyte, and counter electrodes were prepared. The plastisol T/SP as the platinum precursor was coated over the precleaned FTO glass substrate using the doctor blade technique to prepare the counter electrode. Finally, the FTO substrate was annealed for 30 min at 400 °C. The Pt (platinum) coated FTO glass substrate acted as a counter electrode.

The electrolyte solution was synthesized by dissolving iodine (0.127 g) and potassium iodide (0.83 g) in ethylene glycol (10 ml).

Fabrication of DSSCs

The DSSC was fabricated by N719 dye adsorbed FTO/ZnO photoanode, was connected to the top of the Pt counter electrodes, and clamped tightly using binder clips. A drop of the iodide solution (electrolyte) was injected into the two electrodes. The invented device is abbreviated as FTO/ZnO-N719 dye/iodide redox coupled electrolyte/Pt/FTO. The photocurrent measurement was carried out to evaluate the characteristic photovoltaic performance.

Material Characterization

Various characterization methods examined the physicochemical behavior of the synthesized ZnO nanoparticles. The crystalline and structural nature of the prepared ZnO nanoparticles was surveyed by powder PANalytical X-ray diffractometer (CuKα radiation) with λ = 1.5406 Å in 2θ range between 20° to 80°. The functional groups in the synthesized ZnO nanoparticles were analyzed in the spectral range of 500 to 4000 cm^{-1} by PerkinElmer, Waltham, MA, Fourier transform infrared spectroscopy. The absorbance spectra in the wavelength between 200 to 800 nm were monitored by PerkinElmer Lambda 35 UV-visible absorbance spectrophotometer to survey the optical properties. Nanophox Sympatec dynamic light scattering (DLS) investigated the particle size distribution of ZnO. The surface morphology of the ZnO was surveyed by FEI Nova 400 Nano scanning electron microscopy.

RESULTS AND DISCUSSION

XRD Analysis

Figure 1 displays the XRD pattern of prepared ZnO nanoparticles. The sharp deflection peaks located at 31.4°, 34.1°, 35.9°, 47.1°, 56.2°62.5°, 66.1°, 67.7°, 68.9°, 72.2° and 76.6° are indexed to the (100), (002), (101), (102), (110), (103), (200), (112), (201), (004) and (202) crystalline planes, respectively. The detected planes are the distinguishing peaks of the hexagonal wurtzite structure of ZnO nanoparticles well matched with the JCPDS data file (Card No. 89-0510). Moreover, the XRD spectra authenticate that no diffraction peaks of the second phase are recorded, indicating that single-phase ZnO nanoparticles are formed. The sharp diffraction peaks of ZnO nanoparticles suggest their high crystallinity

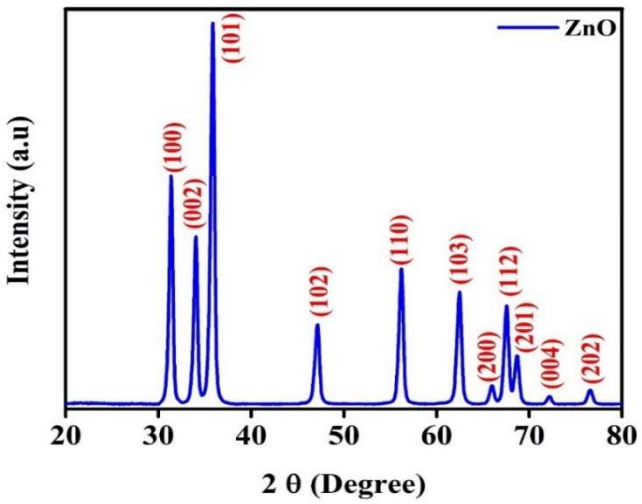

Fig. 1. XRD pattern of synthesized ZnO nanoparticles.

nature. This result agrees well with previously reported literature [30,31]. Debye - Scherrer formula is utilized to estimate the crystallite size by Eq. (1) [32-34]

$$D = \frac{k\lambda}{\beta \cos\theta} \tag{1}$$

Where D denotes the crystallite size, β refers to FWHM of the deflection peak, θ is the angle of diffraction (Bragg's angle), k depicts the Scherrer constant (k = 0.9), λ represents X-ray wavelength (λ = 1.5406 Å). The estimated average crystallite size of the prepared ZnO nanoparticles was 16.28 nm.

The interlayer spacing (d) between atoms was assessed through Brass's law relation (2), which is given below [35,36]

$$d = \frac{\lambda}{2\sin\theta} \tag{2}$$

The prepared ZnO nanoparticles' interlayer spacing (d) was 2.242 Å.

Lattice parameters of a, b and c, microstrain (ε), dislocation density (δ), and unit cell volume (V) were estimated from the following Eqs. (3), (4), (5) and (6) [35,37]

$$\frac{1}{d_{hkl}^2} = \frac{4}{3}\left(\frac{h^2 + hk + k^2}{a^2}\right) + \frac{l^2}{c^2} \tag{3}$$

$$\xi = \frac{\beta}{4\tan\theta} \tag{4}$$

$$\delta = \frac{1}{D^2} \tag{5}$$

$$V = \frac{\sqrt{3}}{2} a^2 c \tag{6}$$

The values of lattice constants, a = b = 3.241 Å and c = 5.217 Å, ξ = 1.235 × 10^{-3} lines^2/m^4, δ = 3.77 × 10^{15} lines/m^2 and V = 47.46 Å^3 are prepared ZnO nanoparticles.

FTIR Analysis

The FTIR spectrum of synthesized ZnO nanoparticles is represented in Fig. 2. The fingerprint region of Zn-O stretching mode vibration appeared at 570 cm^{-1} [38]. Figure 2 authorizes the formation of ZnO in the hexagonal crystalline phase. The mode at 1378 cm^{-1} is indexed as C=O carboxyl group stretching vibration, owing to roughly organic traces from the citrus lemon extract [24]. The bending mode vibration of O-H is noticed at 1620 cm^{-1}. Furthermore, the less intense mode (2856 cm^{-1} and 2922 cm^{-1}) and broadband at 3449 cm^{-1} appeared, which is predictable to the O-H stretching vibration of hydroxyl groups [39]. Hence, this analysis justifies the single phase of ZnO nanoparticles in the prepared samples.

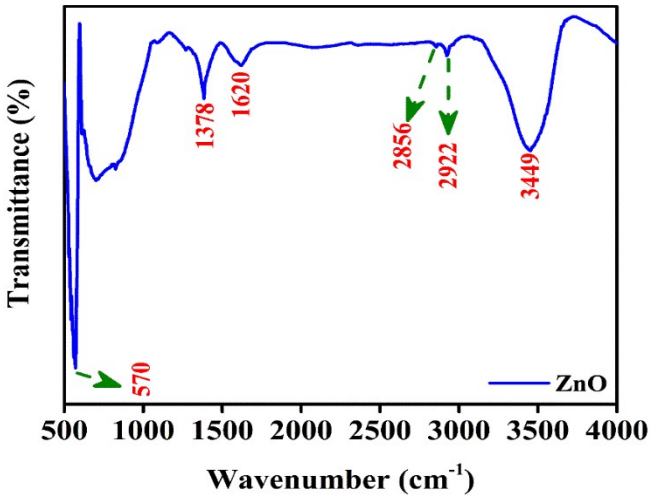

Fig. 2. FTIR spectra of synthesized ZnO nanoparticles.

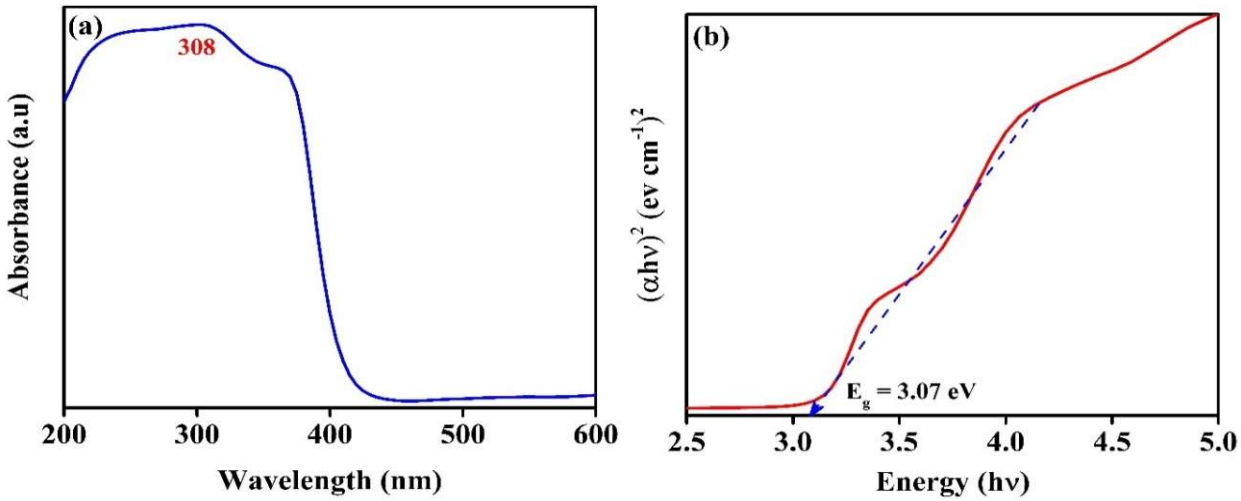

Fig. 3. UV-Vis (a) absorbance spectra. (b) Tauc's plot of ZnO Nanoparticles.

UV-Vis Analysis

The UV-Vis absorption spectrum of the prepared ZnO nanoparticles is depicted in Fig. 3a. It is clear from the range with high transparency in the visible light sector (~400 to 600 nm) and strong absorption in the ultraviolet sector (~200 to 400 nm). Figure 3a shows a prominent exciton absorption band observed at 308 nm, characteristic of highly crystalline ZnO. The blue shift in the absorption band (308 nm) of the prepared ZnO nanoparticles compared to the bulk ZnO (358 nm) suggests that more diminutive than the Bohr radius of the exciton [40]. No other absorption peaks were noticed, confirming the high purity of the synthesized ZnO nanoparticles. The obtained result is well-matched with the previous report.

The energy gap (band gap) of the ZnO was estimated using the Tau-plot relation (7) [41,42]

$$(\alpha h\upsilon)^2 = \beta(h\upsilon - E_g) \quad (7)$$

Where, h, E_g, β, α, and υ represent Planck's constant (6.626×10^{-31} m^2 kg s^{-1}), band gap, proportionality constant, absorption coefficient, and photon frequency, respectively. The value of E_g was assessed from the plot (see Fig. 3b) among hυ and $(\alpha h\upsilon)^2$. The E_g was estimated from Fig. 3b at 3.07 eV. It is vital to observe that E_g's values are smaller than the previously reported data of ZnO (3.37 eV). As a result, the blue shift in the E_g can be ascribed to quantum confinement effects, and the electron is quickly excited from the VB (valence band) to the CB (conduction band) due to the smaller E_g.

DLS Analysis

DLS analysis was shown to measure the size and distribution of the prepared ZnO nanoparticles. The size distribution spectrum (DLS) of the ZnO nanoparticle is represented in Fig. 4. It signifies that the distributed particle size is 7 nm (d_{10}) to 53 nm (d_{50}). From Fig. 4, it was validated that all sizes of the particles in the nano regime for the synthesized ZnO nanoparticles and the result following SEM analysis.

SEM Analysis

Figure 5 depicts the surface morphology of prepared ZnO nanoparticles. The SEM image revealed the spherical shape with uniformly distributed ZnO nanosize particles with a particle size of ~45 nm. Besides, fewer agglomerated nanoparticles are noticed.

Photovoltaic Performance

The photovoltaic behaviors of the invented DSSC devices with FTO/ZnO-N719 dye/iodide redox coupled electrolyte/Pt/FTO are monitored through the J (current density) as a function of V (applied voltage). The fabricated

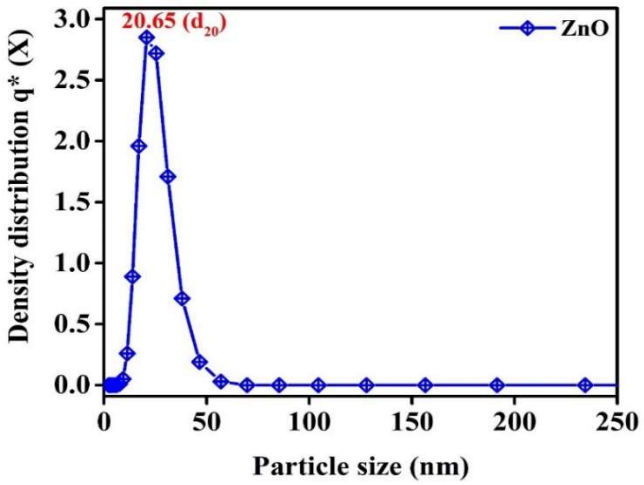

Fig. 4. DLS particle distribution spectrum of synthesized ZnO nanoparticles.

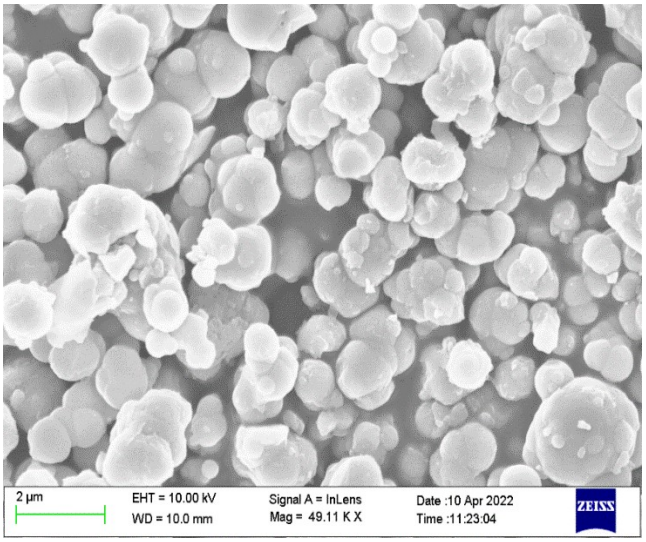

Fig. 5. SEM images of ZnO nanoparticles.

DSSC architecture consists of synthesized ZnO semiconductor nanoparticles as a photoanode, N719 ruthenium dye used as a sensitizer, I_3^-/I^- redox electrolyte for boosting the redox couple regeneration and reducing oxidized dye and platinum (Pt) is operated as a counter electrode. The performance of the fabricated device is tested under simulated sunlight with intensities of 100 mW cm^{-2}. The active area of the FTO substrate was 1 cm^2. The J-V curve of the constructed DSSCs is shown in Fig. 6. The

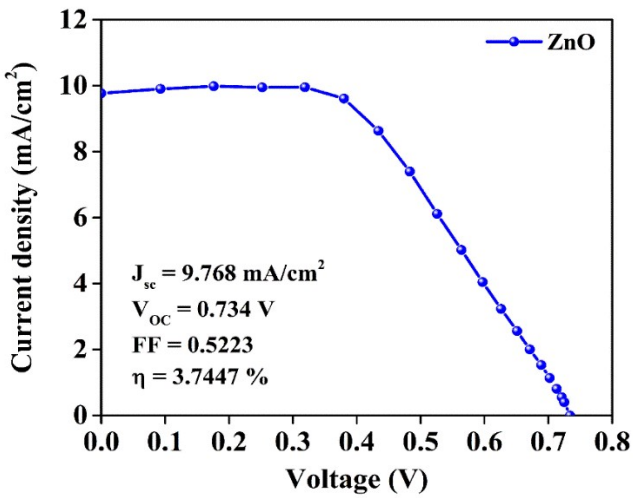

Fig. 6. J-V curve for the DSSCs with ZnO as photoanode material.

detailed photovoltaic performance characteristics like J_{sc} (short-circuit current density), η (power conversion efficiency), *FF* (fill factor), and V_{oc} (open-circuit voltage) are estimated. The "*FF*" and "η" of the fabricated DSSC device can be obtained from Eqs. (8) and (9), respectively [8,27].

$$FF = \frac{J_{max} \times V_{max}}{J_{sc} \times V_{oc}} \tag{8}$$

$$\eta = \frac{J_{sc} \times V_{oc} \times FF}{P_{in}} \tag{9}$$

Where V_{max} is the maximum voltage, J_{sc} is the short circuit photocurrent density, J_{max} is the maximum current density, and P_{in} is the power of incident radiation (mA cm^{-2}), V_{oc} is the open circuit photovoltage. It is observed that the fabricated device exhibited *J*sc is 9.768 mA cm^{-2} and V_{oc} is 0.734 V with FF of 0.5223, leading to the conversion efficiency (η) of 3.7447%. The η of the present study is greater than the data reported in the previous literature. For example, the ZnO nanoflower photoanode exhibits 1.0% [43]. Bundle-like ZnO nanorods showed an of 1.38% [44]. Chatterjee *et al.* [45] achieved 1.56% in ZnO nanorods. ZnO rods synthesized by a hydrothermal route exhibited 1.62% [46]. Hence, the obtained photovoltaic characteristics of DSSCs such as FF and ZnO nanoparticles as photoanode

confirm the superior power conversion efficiency compared to the formerly published literature.

CONCLUSION

The present research demonstrates the preparation of ZnO nanoparticles via a green, facile solution combustion method and is utilized as a photoanode material to construct the DSSC. XRD, FTIR, UV-Vis, DLS, and SEM studied the crystallinity, functional group, surface morphology, optical properties, and band gap. The XRD confirms the ZnO nanoparticles' pure single-phase wurtzite hexagonal structure; no secondary phases were presented. The average crystallite size (D = 16.28 nm), interlayer spacing (d = 2.242 Å), lattice constants [a = b = 3.241 Å and c = 5.217 Å], dislocation density ($\delta = 3.77 \times 10^{15}$ lines/m^2), microstrain ($\varepsilon = 1.235 \times 10^{-3}$ lines^2/m^4) and unit cell volume (V = 47.46 Å^3) were estimated. The E_g (Bandgap) of the ZnO nanoparticles was estimated as 3.07 eV via Tau Plot. The SEM image reveals the spherical ZnO nanoparticles in homogenous form with a particle size of ~50 nm. The DSSC was built with the structure of FTO/ZnO-N719 dye/iodide redox couple electrolyte/Pt/FTO. The photovoltaic characteristic, such as J_{sc}, V_{oc}, and *FF,* was estimated to be 9.768 mA cm^{-2}, 0.734 V, and 05.223 respectively. A maximum photovoltaic conversion efficiency, PCE (η) of 3.7447%, was reached for the fabricated DSSC under standard sun illumination (100 mW cm^{-2}). The synthesis route is crucial for preparing photo anode to construct more efficient photoelectric conversion efficiency DSSCs. Hence, the prepared ZnO nanoparticles may serve as an excellent photoanode material for DSSCs applications.

REFERENCES

[1] Zhang, L.; Cole J. M.; Anchoring Groups for Dye-Sensitized Solar Cells. *ACS Appl. Mater. Interfaces* **2015**, *7* (6), 3427-3455, DOI: 10.1021/am507334m.

[2] Manjula, N.; Chen, S. -M.; One-pot synthesis of rod-shaped gadolinia doped zinc oxide decorated on graphene oxide composite as an efficient electrode material for isoprenaline sensor. *Compos. B. Eng.* **2021**, *211*, 108631, DOI: 10.1016/ j.compositesb.2021.108631.

[3] Sugathan, V.; John E.; Sudhakar, K.; Recent improvements in dye-sensitized solar cells: A review. *Renewable and Sustainable Energy Rev.* **2015**, *52*, 54-64, DOI: 10.1016/j.rser.2015.07.076.

[4] Sun, L.; Shao, Q.; Zhang, Y.; Jiang, H.; Ge, S.; Lou, S.; Lin, J.; Zhang, J.; Wu, S.; Dong, M.; Guo, Z., N self-doped ZnO derived from microwave hydrothermal synthesized zeolitic imidazolate framework-8 toward enhanced photocatalytic degradation of methylene blue. *J. Colloid Interface Sci.* **2020**, *565*, 142-155, DOI: 10.1016/j.jcis.2019.12.107.

[5] Shashanka, R.; Esgin, H.; Yilmaz, V. M.; Caglar, Y., Fabrication and characterization of green synthesized ZnO nanoparticle based dye-sensitized solar cells. *J. Sci.: Adv. Mater. Devices* **2020**, *5* (2), 185-191, DOI: 10.1016/j.jsamd.2020.04.005.

[6] Shashanka, R.; Kamacı, Y.; Taş, R.; Ceylan, Y.; Bülbül, A. S.; Uzun O.; Karaoglanli A. C., Antimicrobial Investigation of CuO and ZnO Nanoparticles Prepared by a Rapid Combustion Method. *Phys. Chem. Res.* **2019**, *7*, 799-812, DOI: 10.22036/ pcr.2019.199338.1669.

[7] Rajendrachari, S.; Taslimi, P.; Karaoglanli, A. C.; Uzun, O.; Alp, E.; Jayaprakash G. K., Photocatalytic degradation of Rhodamine B (RhB) dye in waste water and enzymatic inhibition study using cauliflower shaped ZnO nanoparticles synthesized by a novel One-pot green synthesis method. *Arab. J. Chem.* **2021**, *14*, 103180, DOI: 10.1016/j.arabjc.2021.103180.

[8] Das, D.; Makal, P., CdS Q-Dot-Impregnated TiO_2-B Nanowire-Based Photoanodes for Efficient Photovoltaic Conversion in 'Q-Dot Co-sensitized DSSC. *Energy & Fuels* **2021**, *35* (9), 8246-8262, DOI: 10.1021/acs.energyfuels.1c00539.

[9] O'Regan, B.; Grätzel, M.; A low-cost, high-efficiency solar cell based on dye-sensitized colloidal TiO_2 films. *Nature* **1991**, *353* (6346), 737-740, DOI: 10.1038/ 353737a0.

[10] Benazzi, E.; Mallows, J.; Summers, G. H.; Black, F. A.; Gibson, E. A., Developing photocathode materials for p-type dye-sensitized solar cells. *J. Mater. Chem. C* **2019**, *7* (34), 10409-10445, DOI: 10.1039/ C9TC01822K.

[11] Sharma, K.; Sharma, V.; Sharma, S. S., Dye-Sensitized

Solar Cells: Fundamentals and Current Status. *Nanoscale Res. Lett.* **2018**, *13* (1), 381, DOI: 10.1186/s11671-018-2760-6.

[12] Mathew, S.; Yella, A.; Gao, P.; Humphry-Baker, R.; Curchod, B. F. E.; Ashari-Astani, N.; Tavernelli, I.; Rothlisberger, U.; Nazeeruddin, M. K.; Grätzel, M., Dye-sensitized solar cells with 13% efficiency achieved through the molecular engineering of porphyrin sensitizers. *Nature Chem.* **2014**, *6* (3), 242-247, DOI: 10.1038/nchem.1861.

[13] Wibowo, A.; Marsudi, M. A.; Amal, M. I.; Ananda, M. B.; Stephanie, R.; Ardy, H.; Diguna, L. J.; ZnO nanostructured materials for emerging solar cell applications. *RSC Adv.* **2020**, *10* (70), 42838-42859, DOI: 10.1039/D0RA07689A.

[14] Han, J.; Fan, F.; Xu, C.; Lin, S.; Wei, M.; Duan, X.; Wang, Z. L., ZnO nanotube-based dye-sensitized solar cell and its application in self-powered devices. *Nanotechnology* **2010**, *21* (40), 405203, DOI: 10.1088/0957-4484/21/40/405203.

[15] Keis, K.; Magnusson, E.; Lindstrom, H.; Lindquist, S.-E.; Hagfeldt, A., A 5% Efficient Photo Electrochemical Solar Cell Based on Nanostructured ZnO Electrodes. *Sol. Energy Mater. Sol. Cells* **2002,** *73*, 51-58, DOI: 10.1016/S0927-0248(01)00110-6.

[16] Li, Z.; Zhou, Y.; Xue, G.; Yu, T.; Liu, J.; Zou, Z., Fabrication of hierarchically assembled microspheres consisting of nanoporous ZnO nanosheets for high-efficiency dye-sensitized solar cells. *J. Mater. Chem.* **2012**, *22* (29), 14341-14345, DOI: 10.1039/C2JM32823B.

[17] Liang, F. -X.; Gao, Y.; Xie, C.; Tong, X. -W.; Li, Z. -J.; Luo, L. -B., Recent advances in the fabrication of graphene-ZnO heterojunctions for optoelectronic device applications. *J. Mater. Chem. C* **2018**, *6* (15), 3815-3833, DOI: 10.1039/C8TC00172C.

[18] Shashanka, R., Investigation of optical and thermal properties of CuO and ZnO nanoparticles prepared by Crocus Sativus (Safron) fower extract. *J. Iran. Chem. Soc.* **2021**, *18*, 415-427, DOI: 10.1007/s13738-020-02037-3.

[19] Shashanka, R.; Yilmaz, V. M.; Karaoglanli, A. C.; Uzun, O., Investigation of activation energy and antibacterial activity of CuO nanorods prepared by Tilia Tomentosa (Ihlamur) leaves. *Mor. J. Chem.* **2020**, *8*, 497-509. DOI: 10.48317/IMIST.PRSM/morjchem-v8i2.17765.

[20] Pandith, A.; Jayaprakash, G. K.; ALOthman, Z. A.; Surface-modified CuO nanoparticles for photocatalysis and highly efficient energy storage devices. *Environ. Sci. Pollut. Res.* **2023**, *30*, 43320-43330, DOI: 10.1007/s11356-023-25131-4.

[21] Rajendrachari, S.; Jayaprakash, G. K.; Pandith, A.; Karaoglanli, A. C.; Uzun, O., Electrocatalytic Investigation by Improving the Charge Kinetics between Carbon Electrodes and Dopamine Using Bio-Synthesized CuO Nanoparticles. *Catalysts* **2022**, *12*, 994, DOI: 10.3390/catal12090994.

[22] Nagarajarao, S. H.; Nandagudi, A.; Viswanatha, R.; Basavaraja, B. M.; Santosh, M.S.; Praveen, B. M.; Pandith, A., Recent Developments in Supercapacitor Electrodes: A Mini Review. *ChemEngineering* **2022**, *6*, 5, DOI: 10.3390/chemengineering6010005.

[23] Banu, R.; Swamy, B. E. K.; Pandith, A., A Selective Electrochemical Sensing of Serotonin and Epinephrine at Glassy Carbon Electrode Modulated with Brilliant Green: A Voltammetric Study. *Curr. Anal. Chem.* **2023**, *19*, 339-347, DOI: 10.2174/1573411019666230418093328

[24] Gowthambabu, V.; Balamurugan, A.; Bharathy, R. D.; Satheeshkumar S.; Kanmani S. S., ZnO nanoparticles as efficient sunlight driven photocatalyst prepared by solution combustion method involved lime juice as biofuel. *Spectrochim. Acta A Mol. Biomol. Spectrosc.* **2021**, *258*, 119857, DOI: 10.1016/j.saa.2021.119857.

[25] Tarwal, N. L.; Jadhav, P. R.; Vanalakar, S. A.; Kalagi, S. S.; Pawar, R. C.; Shaikh, J. S.; Mali, S. S.; Dalavi, D. S.; Shinde, P. S.; Patil, P. S., Photoluminescence of zinc oxide nanopowder synthesized by a combustion method. *Powder Technol.* **2011**, *208*, 185-188, DOI: 10.1016/j.powtec.2010.12.017.

[26] Krishna, P. G.; Ananthaswamy, P. P.; Trivedi, P.; Chaturvedi, V.; Mutta, N. B.; Sannaiah, A.; Erra, A.; Yadavalli, T., Antitubercular activity of ZnO nanoparticles prepared by solution combustion synthesis using lemon juice as bio-fuel. *Mater. Sci. Eng. C.* **2017**, *75*, 1026-1033, DOI: 10.1016/j.msec.2017.02.093.

[27] Gowthambabu, V.; Deshpande, M.; Govindaraj, R.; Krishna, V. K. N.; Charumathi, M. L.; Kumar, J. M.; Vignesh, M. S. D.; Isaac Daniel, R.; Ramasamy, P., Synthesis of anatase TiO_2 microspheres and their efficient performance in dye-sensitized solar cell. *J. Mater. Sci.: Mater. Electron.* **2021**, *32* (22), 26306-26317, DOI: 10.1007/s10854-021-06923-1

[28] Dubey, R. S.; Jadkar, S. R.; Bhorde A. B., Synthesis and Characterization of Various Doped TiO_2 Nanocrystals for Dye-Sensitized Solar Cells. *ACS Omega* **2021**, *6*, 3470-3482, DOI: 10.1021/acsomega.0c01614.

[29] Srinivasan, V.; Sivanadanam, J.; Ramanujam, K.; Jhonsi, M. A., Delineating the enhanced efficiency of carbon nanomaterials including the hierarchical architecture of the photoanode of dye-sensitized solar cells. *Mater. Adv.* **2020**, *1*, 2964-2970, DOI: 10.1039/d0ma00654h.

[30] Muhammad, W.; Ullah, N.; Haroon, M.; Abbasi, B. H., Optical, morphological and biological analysis of zinc oxide nanoparticles (ZnO NPs) using Papaver somniferum L. *RSC Adv.* **2019**, *9* (51), 29541-29548, DOI: 10.1039/C9RA04424H.

[31] Zak, A. K.; Razali, R.W.H.; Darroudi, A. M.; Synthesis and characterization of a narrow size distribution of zinc oxide nanoparticles. *Int. J. Nanomedicine* **2011**, *6*, 1399-1403, DOI: 10.2147/IJN.S19693.

[32] Muthu, R. N.; Tatiparti, S. S. V., Electrochemical Behavior of Cobalt Oxide/Boron-Incorporated Reduced Graphene Oxide Nanocomposite Electrode for Supercapacitor Applications. *J. of Materi. Eng. and Perform.* **2020**, *29* (10), 6535-6549, DOI: 10.1007/s11665-020-05176-z.

[33] Muthu, R. N.; Tatiparti, S. S. V., Electrode and symmetric supercapacitor device performance of boron-incorporated reduced graphene oxide synthesized by electrochemical exfoliation. Energy Storage **2020**, *2* (4), e134, DOI: 10.1002/est2.134.

[34] Shashanka, R.; Jayaprakash, G. K.; Prakashaiah, B. G.; Kumar, M.; Swamy, B. E. K., Electrocatalytic determination of ascorbic acid using a green synthesized magnetite nano-flake modified carbon paste electrode by cyclic voltammetric method. *Mater. Res. Innov.* **2022**, *26*, 229-239, DOI: 10.1080/14328917.2021.1945795.

[35] Saleem, S.; Jameel, M. H.; Rehman, A.; Tahir, M. B.; Irshad, M. I.; Jiang, Z. -Y.; *et al.*, Evaluation of structural, morphological, optical, and electrical properties of zinc oxide semiconductor nanoparticles with microwave plasma treatment for electronic device applications. *J. Mater. Sci. Technol.* **2022**, *19*, 2126-2134, DOI: 10.1016/j.jmrt.2022.05.190.

[36] Shashankaa, R.; Swamy, B. E. K., Biosynthesis of Silver Nanoparticles Using Leaves of Acacia Melanoxylon and their Application as Dopamine and Hydrogen Peroxide Sensors. *Phys. Chem. Res.*, **2020**, *8*, 1-18, DOI: 10.22036/pcr.2019.205211.1688.

[37] Rajendrachari, S.; Jayaprakash, G. K.; Pandith, A.; Karaoglanli, A. C.; Uzun O., Electrocatalytic Investigation by Improving the Charge Kinetics between Carbon Electrodes and Dopamine Using Bio-Synthesized CuO Nanoparticles. *Catalysts* **2022**, *12*, 994, DOI: 10.3390/catal12090994.

[38] Mahalakshmi, S.; Hema, N.; Vijaya, P. P., *In Vitro* Biocompatibility and Antimicrobial activities of Zinc Oxide Nanoparticles (ZnO NPs) Prepared by Chemical and Green Synthetic Route-A Comparative Study. *BioNanoScience* **2020**, *10*, DOI: 10.1007/s12668-019-00698-w.

[39] Faisal, S.; Jan, H.; Shah, S. A.; Shah, S.; Khan, A.; Akbar, M. T.; Rizwan, M.; Jan, F.; WajidullahAkhtar, N.; Khattak, A.; Syed, S., Green Synthesis of Zinc Oxide (ZnO) Nanoparticles Using Aqueous Fruit Extracts of Myristica fragrans: Their Characterizations and Biological and Environmental Applications. *ACS Omega* **2021**, *6* (14), 9709-9722, DOI: 10.1021/acsomega.1c00310.

[40] Arefi, M.; Rezaei-Zarchi, S., Synthesis of Zinc Oxide Nanoparticles and Their Effect on the Compressive Strength and Setting Time of Self-Compacted Concrete Paste as Cementitious Composites. *Int. J. Mol. Sci.* **2012**, *13*, 4340-50, DOI: 10.3390/ijms13044340.

[41] Pogacean, F.; Stefan, M.; Toloman, D.; Popa, A.; Leostean, C.; Ioan- Alexandru, T.; Coroş, M.; Pana, O.; Pruneanu, S., Photocatalytic and Electrocatalytic Properties of NGr-ZnO Hybrid Materials. *Nanomaterials* **2020,** *10*, 1473, DOI: 10.3390/nano10081473.

[42] Rajendrachari, S.; Karaoglanli, A. C.; Ceylan, Y.; Uzun

O., A Fast and Robust Approach for the Green Synthesis of Spherical Magnetite (Fe_3O_4) Nanoparticles by Tilia tomentosa (Ihlamur) Leaves and its Antibacterial Studies. *Pharm. Sci.* **2020**, *26*, 175-183, DOI: 10.34172/PS.2020.5

[43] Jiang, C. Y.; Sun, X. W.; Lo, G. Q.; Kwong, D. L.; Wang, J. X., Improved dye-sensitized solar cells with a ZnO-nanoflower photoanode. *Appl. Phys. Lett.* **2007**, *90* (26), 263501, DOI: 10.1063/1.2751588.

[44] Zhang, Q.; Hou, S.; Li, C., Titanium Dioxide-Coated Zinc Oxide Nanorods as an Efficient Photoelectrode in Dye-Sensitized Solar Cells. *Nanomaterials* **2020**, *10* (8), 1598, DOI: 10.3390/nano10081598.

[45] Chatterjee, S.; Performance of Dye-Sensitized Solar Cells (DSSCs) Fabricated with Zinc Oxide (ZnO) Nanpowders and Nanorods. *J. of Materi. Eng. and Perform.* **2018**, *27* (6), 2713-2718, DOI: 10.1007/s11665-018-3285-y.

[46] Kumar, V.; Gupta, R.; Bansal, A., Hydrothermal Growth of ZnO Nanorods for Use in Dye-Sensitized Solar Cells. *ACS Appl. Nano Mater.* **2021**, *4* (6), 6212-6222, DOI: 10.1021/acsanm.1c01012.